Cyclic Breathing Simulations in Large-Scale Models of the Lung Airway From the Oronasal Opening to the Terminal Bronchioles

D. Keith Walters
Department of Mechanical Engineering,
Mississippi State University,
Starkville, MS 39762

Greg W. Burgreen
CAVS SimCenter,
Mississippi State University,
Starkville, MS 39762

Robert L. Hester
Department of Physiology,
University of Mississippi Medical Center,
Jackson, MS 39216

David S. Thompson
Department of Aerospace Engineering,
Mississippi State University,
Starkville, MS 39762

David M. Lavallee
Department of Aerospace Engineering,
Mississippi State University,
Starkville, MS 39762

William A. Pruett
Department of Physiology,
University of Mississippi Medical Center,
Jackson, MS 39216

Xiao Wang
CAVS SimCenter,
Mississippi State University,
Starkville, MS 39762

Computational fluid dynamics (CFD) simulations were performed using large-scale models of the human lung airway and unsteady periodic breathing conditions. The computational domain included fully coupled representations of the orotracheal region and large conducting zone up to generation four (G4) obtained from patient-specific CT data, and the small conducting zone (to the 16th generation) obtained from a stochastically generated airway tree with statistically realistic morphological characteristics. A reduced-geometry airway model was used, in which several airway branches in each generation were truncated, and only select flow paths were retained to the 16th generation. The inlet and outlet flow boundaries corresponded to the oral opening, the physical inlet/outlet boundaries at the terminal bronchioles, and the unresolved airway boundaries created from the truncation procedure. The total flow rate was specified according to the expected ventilation pattern for a healthy adult male, which was supplied by the whole-body modeling software HumMod. The unsteady mass flow distribution at the distal boundaries was prescribed based on a preliminary steady-state simulation with an applied flow rate equal to the average flow rate during the inhalation phase of the breathing cycle. In contrast to existing studies, this approach allows fully coupled simulation of the entire conducting zone, with no need to specify distal mass flow or pressure boundary conditions a priori, and without the use of impedance or one-dimensional (1D) flow models downstream of the truncated boundaries. The results show that: (1) physiologically realistic flow is obtained in the model, in terms of cyclic mass conservation and approximately uniform pressure distribution in the distal airways; (2) the predicted alveolar pressure is in good agreement with correlated experimental data; and (3) the use of reduced-order geometry modeling allows accurate and efficient simulation of large-scale breathing lung flow, provided care is taken to use a physiologically realistic geometry and to properly address the unsteady boundary conditions. [DOI: 10.1115/1.4027485]

Introduction

Predicting air flow in the human lung using computational fluid dynamics (CFD) is complicated by several factors, including the need for an anatomically correct computational geometry, the overall size and complexity of the lung airway, and the time-dependent nature of the flowfield during cyclic breathing. The first of these difficulties has recently been addressed through the use of computerized tomography (CT) scans to create anatomical models that incorporate locally accurate details of the geometry of the upper airways [1,2], or provide lobe structure and morphological statistics that can be used to create realistic approximations of the lower airways [3]. For example, several studies have made use of stochastically generated airway trees to approximate realistic anatomies in a statistical sense, and a number of simulations have been performed using fully resolved models for some number of upper generations of the airway (e.g., [4–6]). Stochastically generated, anatomically realistic models have also been used as a basis for semianalytical solutions of airway resistance and particle deposition in the conducting zone [7–9], and for CFD simulations of particle transport and deposition in acinar airway regions [10]. The current state-of-the-art in lung geometry modeling combines both of these approaches to develop subject-specific, physiologically realistic models of the airway tree from the extrathoracic regions to the terminal bronchioles, i.e., the conducting zone of the human lung [11].

At present, three-dimensional Navier–Stokes CFD simulations in fully resolved computational models of the conducting zone are intractable due to the large number (~64 K) of airway branches that need to be resolved [12,13]. As a consequence, most CFD studies to date have focused only on relatively small subsections of the bronchopulmonary tree. For the relatively few large-scale simulations documented in the literature, two simplifying approaches that have been adopted are sequential simulation and reduced-geometry modeling. In the former, simulations are performed in successively smaller (during inhalation) or larger (during exhalation) subsections of the geometry, with outlet conditions from one simulation providing the inlet conditions for the next simulation [14,15]. The study by Nowak et al. [14] modeled particle deposition during cyclic breathing, up to generation 12, by successively simulating only a small portion of the unsteady breathing cycle in each of the subsections.

Reduced-geometry models, in contrast, allow fully coupled, simultaneous simulation in all resolved regions of the simulation

Contributed by the Fluids Engineering Division of ASME for publication in the JOURNAL OF FLUIDS ENGINEERING. Manuscript received January 29, 2013; final manuscript received April 21, 2014; published online July 24, 2014. Assoc. Editor: Francine Battaglia.

domain. In this approach, only a portion of the overall airway geometry is retained in the computational model. This approach has been shown to provide accurate predictions of airflow characteristics and inhaled particle deposition in idealized airway trees under steady-state flow conditions [12,16]. Furthermore, the reduced geometry approach has been coupled with realistic, CT-scan-based computational geometries to provide realistic yet efficient CFD models for steady-state inhalation [17]. Recent studies have adopted the most limiting case of a reduced-geometry approach, in which a single flow path is modeled as a representative example of the flow through all investigated generations of airflow [18–21].

Figure 1 provides an illustration of the reduced-geometry approach, based on truncation of selected airway branches. Figure 1(*a*) shows a fully resolved representation of an idealized nine-generation bronchial tree, with symmetric branching based on the well known Weibel [22] morphology. An example of a corresponding reduced geometry is shown in Fig. 1(*b*). The reduced geometry is created by removing (truncating) 50% of the airway paths in each generation beyond generation 2 (G2), where G0 represents the largest airway branch. The resulting approximation consists of four individual flow paths extending from G0 to G8. Assuming that each airway bifurcation unit contains approximately the same number of mesh points, truncation reduces the model mesh size by approximately 98%. However, the truncation process also produces unresolved airway flow boundaries in each of the generations between G2 and G8. In order to obtain reasonable results from a reduced-geometry model, it is necessary to apply physiologically realistic boundary conditions at these truncated boundaries.

Among studies employing reduced-geometry models, five different approaches can be identified for specification of boundary conditions at truncated airway boundaries. These may be summarized as: specified pressure [23], specified mass flow rate [18–21,24], impedance modeling [25,26], 1D modeling of truncated branches [11,13], and stochastic coupling of interior and outlet zones [12,16,17]. The first two approaches are self-explanatory. The third employs a linear or nonlinear relationship between pressure and flow rate at the truncated boundary, which is typically based on a zero-dimensional (0D) electrical transmission line model of the remainder of the airway tree extending from the truncated boundary to the terminal generation. The flow in the 0D model is computed using assumed values for resistance, capacitance, and conductance of each airway branch. The fourth method retains the lower airway branches in the geometrical model, discretized only in the airflow direction, and adopts a local relationship between pressure drop and flow rate, usually by analogy to Poiseuille flow. The fifth method was proposed as an alternative to the above approaches, and was shown using the idealized geometry in Fig. 1 to yield results that are quantitatively similar to those obtained using a fully resolved model [12,16]. Briefly, this approach randomly maps the pressure at resolved interior locations in a particular generation of the airway tree to unresolved outlet locations within the same generation. Unresolved outlet pressures therefore converge toward constant values as the simulation proceeds. The method allows fully coupled simulation over all morphological scales, eliminates the need for a priori prescription of pressure, flow rate, or impedance at truncated outlet boundaries, and does not require coupling between three-dimensional (3D) CFD and 1D flow resistance models.

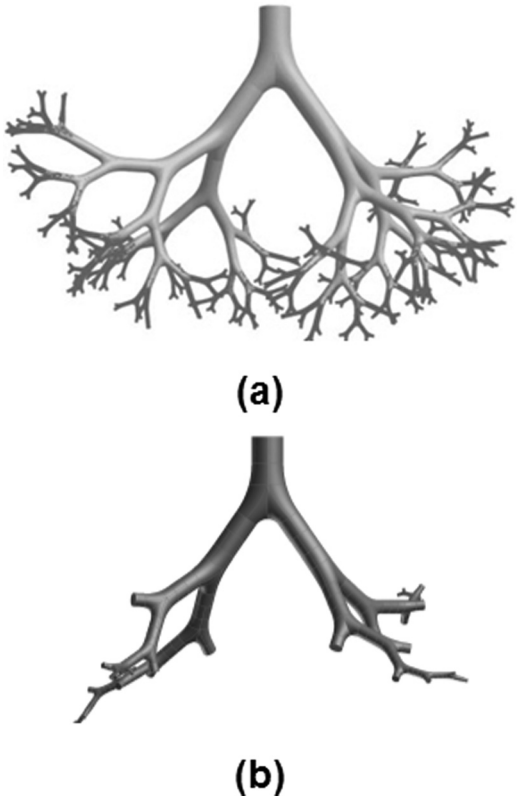

Fig. 1 Illustration of fully resolved (*a*) versus truncated and (*b*) model geometries for CFD simulations of the flow in lung airway branching networks

For unsteady breathing simulations, there is the added difficulty of time dependency with regard to providing physiologically appropriate boundary conditions for the physical (i.e., nontruncated) boundaries. Two obvious approaches for normal breathing states are to use cyclic pressure conditions at the outlets of the distal airways, or to enforce a priori mass flow profiles at those outlets. The former approach, while acceptable for steady-state simulations, cannot guarantee that mass is conserved throughout the inhale–exhale cycle. Furthermore, the implementation of purely pressure-driven flow in pressure-based CFD simulations leads to slow propagation of mass flow imbalance errors and, as a consequence, slow convergence rates. In practice, it is more advantageous to specify the mass flow directly, either at the oral opening (a flow inlet during inhalation) or the distal airway boundaries (flow inlets during exhalation). Tian et al. [18] recently performed simulations for the entire conducting zone (generations 0–16) using a stochastic individual path (SIP) model, in which a single airway flow path was retained down the entire length of the bronchial tree. They successfully simulated transient inhalation by specifying mass flow rate boundary conditions at truncated outlets, based on an assumed even split of the air flow at each bifurcation.

In a recent paper from our group [27], we investigated similar boundary condition treatments, extended for use in a multiple flow path truncated airway model based on a realistic anatomical description [17]. Results were obtained for the full breathing cycle, using a representative ventilation profile for a resting adult male. Three different methods were examined for specifying the mass flow distribution at the outlets, including the assumption of equal mass flow at each bifurcation, the assumption of proportional splitting based on cross-sectional area in each daughter tube, and the assumption of proportional splitting based on the square of the cross-sectional area in each daughter tube. The latter method was based on the result for laminar pressure driven tube flow, for which the pressure gradient is proportional to the area squared. As expected, this method yielded the best results in terms of nearly uniform distal pressures. However, all of the methods suffered from physiologically inaccurate distal pressure distributions (i.e., dramatically different values of pressure at different terminal boundaries), and none of the methods provided good quantitative agreement with expected terminal (i.e., alveolar) pressure levels during breathing.

The current study further investigates simulation of cyclic breathing in reduced-geometry airway models. The key novel

aspect is the presentation of a physiologically realistic method for prescribing air flow distribution at the terminal and truncated distal boundaries, based on a steady state preliminary simulation using stochastically coupled pressure boundary conditions. The method is simple to implement, and requires only the airway geometry and target inhaled air volume profile as inputs, with no need to determine airway pressures at distal boundaries using one-dimensional or impedance-based approximations, and no need to prescribe the mass flow or pressure distribution a priori. The computational geometry was generated using a combination of subject-specific CT-scan data and a space-filling stochastic procedure, based on statistically realistic values for branching angle, branch diameter, and branch length in each generation for the lower airways. Simulations are presented for a full breathing cycle, for flow in the entire conducting zone of the lung, including the oral cavity, trachea, bronchi, and bronchioles up to the 16th generation. Since the breathing flow rate is prescribed as a simulation input, results are interrogated based on distal pressure distributions and overall time-dependent alveolar pressure levels. The major contribution of the present work beyond the previous work of our group [12,16,17,27] is the demonstration of the unsteady breathing simulation methodology for a more realistic geometry obtained using accurate computerized tomography (CT) scans of the upper airways, and a stochastically generated lower airway geometry that is physiologically statistically accurate in terms of relevant geometrical quantities such as airway diameter, branching angle, etc. The paper also expands previous validation and verification by comparing CFD results to those from a whole body physiology simulation tool (HumMod) for several different physiological states, and to available experimental data. The remainder of the paper includes a description of the computational airway model, details of the simulation methodology including boundary condition specification and numerical methods used, presentation of results, and conclusions.

Computational Model

In order to create an accurate oral cavity and throat geometry, the CT-inspired approach described in Ref. [17] was employed. In brief, the commercial software package Mimics (Materialise, Leuven, Belgium) was used to segment and process anonymous CT data of nasopharyngeal passages (Fig. 2). Due to resolution quality issues and small regions of corrupt CT data, the anatomical structure of the oropharynx was manually reconstructed using an in-house geometry tool (SolidMesh [28]), to approximate visible contours in the CT scans. Manual construction of the trachea involved its approximation by a deformed cylindrical shape without cartilaginous rings. Note that the trachea is not a straight cylinder because, in general, it must curve outward to bypass the aorta. The CT-based, manually reconstructed oral cavity and trachea is shown in Fig. 3.

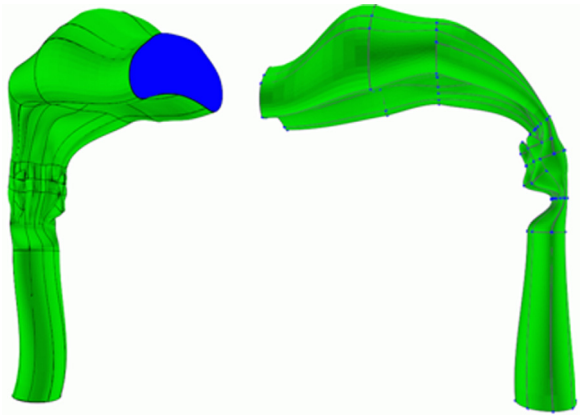

Fig. 3 CT-based, manually generated model of the oral cavity and pharynx regions

The bronchial and bronchiolar regions were generated by randomly selecting airways from a complete bronchial tree dataset that space filled the left and right lungs. A two-step process was undertaken. First, geometry for the upper bronchi region was obtained directly from anonymous CT data of the tracheobronchial airway through four generations. The upper bronchial geometry was merged with the orotracheal geometry described above, as shown in Fig. 4(*a*). Creation of the lower airway skeletal branching was based on an approach inspired by Kitaoka et al. [29] and Tawhai et al. [30] in which morphologically accurate lower airway geometries (i.e., statistically accurate distributions of branch diameters, lengths, and angles) were created within the space constraints of CT extracted lung volumes. Figure 4(*b*) shows lower airway branching through 16 generations (4944 terminal branches) within the left and right lung volumes. The final bronchial tree consisted of a truncated set of randomly selected isolated terminal airways. Based on the selected skeletal branching structure, lower airway surface geometry generation, merging, scaling, and orientation operations were handled via custom methods available within the commercial software package Discrete (Optimal LLC, Starkville, MS). The lower airway model was then appended to the upper orotracheal geometry. The final composite lung geometry is shown in Fig. 5 and consisted of one upper flow boundary (the mouth), 8 main airway pathways, 16 terminal flow outlets, and 165 dichotomous airway bifurcations. All eight of the airway paths extended through 16 generations, representing the physical extent of the conducting zone for the reduced geometry

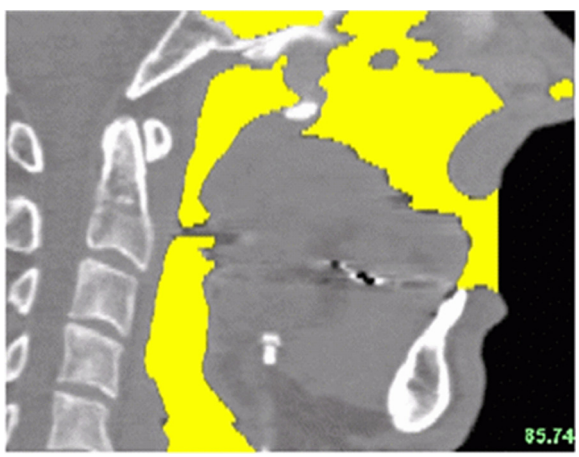

Fig. 2 Example CT image, including airway passage definition (in yellow), used to create upper airway geometry

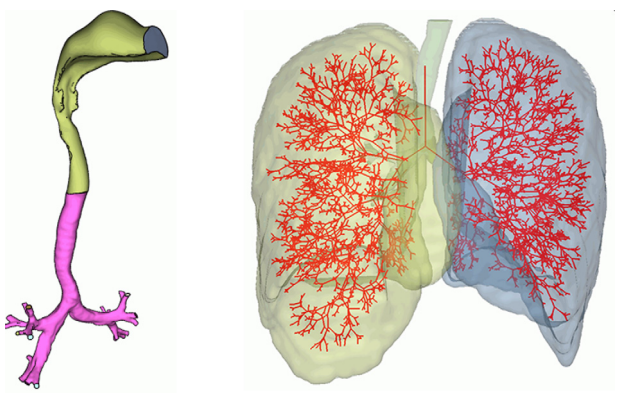

Fig. 4 Upper bronchi branching geometry obtained from CT-scan data (*a*), and skeletonized illustration of space-filling lower airway geometry to 16 generations in left and right lung volumes (*b*)

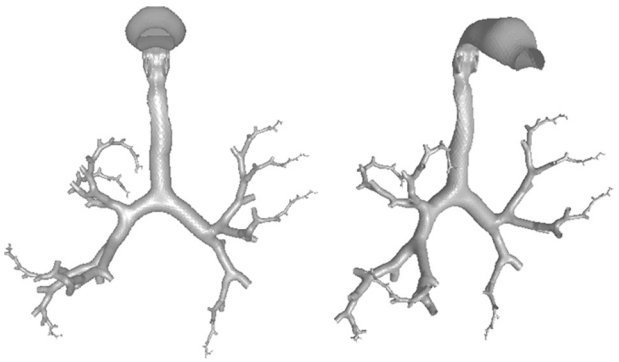

Fig. 5 Final reduced geometry model (Geometry A) comprised of eight distinct flow paths and 16 distal boundaries corresponding to terminal bronchioles (generation 16)

model. All other flow boundaries were denoted as truncated outlets, and were present in generations 5–15. The dimensions of each individual airway were carefully controlled to match values reported in the literature. For example, the flow outlets in generation 16 had mean diameters of 638 μm, in good agreement with documented airway sizes [31]. The overall dimensions of this patient-specific upper airway model were 25.9 cm (vertical) × 22.4 cm (lateral) × 13.5 cm (front-to-back), and the total model volume was 90.4 cm^3. The truncated airway geometry depicted in Fig. 5 is available for download at http://www.digitallung.org.

For comparison purposes, an alternative lower airway model was created using the bronchial tree dataset of Schmidt et al. [32], which is publicly available. This geometry was used in a previous study from our group [17]. The complete airway tree is shown in skeletonized form in Fig. 6(*a*). A corresponding truncated model of the lower airway region was created by random removal of a select number of airway branches at each generation, and the result is shown in Fig. 6(*b*). This alternative truncated geometry contained 141 airflow boundaries, not including the oral opening, of which 135 were unresolved (i.e., truncated boundaries). The six remaining boundaries were considered to be terminal boundaries corresponding to the limit of the conducting zone in the lung. An analysis of the mean airway diameters at each generation showed good agreement with experimental averages that have been reported in the literature [31]. The overall dimensions of this patient-specific upper airway model were 21.8 cm (vertical) × 16.7 cm (lateral) × 13.2 cm (front-to-back), and the total model volume was 29.7 cm^3. For presentation of results in this paper, the geometry created using a stochastically generated lower airway tree, and illustrated in Fig. 5, will be denoted as Geometry A. The alternative geometry, created using the airway tree available in the literature [32] and illustrated in Fig. 6, will be denoted as Geometry B.

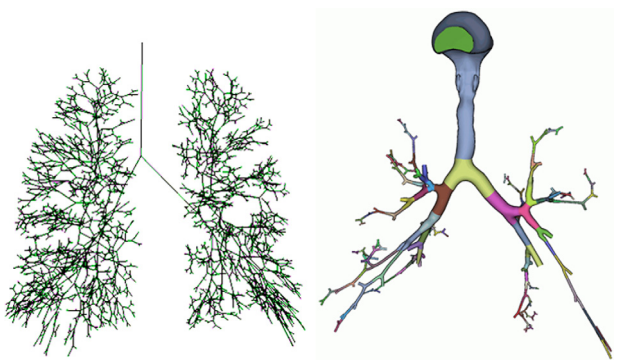

Fig. 6 Alternative reduced geometry model (Geometry B): (*a*) Skeletonized airway tree depicting the lower airway dataset of Schmidt et al. [32] and (*b*) final reduced geometry model

It should be pointed out that a fully realized dichotomous branching model through 16 generations would contain $2^{16}-1$ individual airway segments. In contrast, the eight pathway truncated model used in this study contained 332 segments. It is therefore estimated that the truncated model reduces the computational expense by 99.5% from a fully resolved three-dimensional CFD simulation. For comparison, the 18-generation simulations reported in Gemci et al. [23] were based on the full Schmidt et al. [32] dataset and contained 1453 flow segments.

This study used meshes similar to that in Ref. [17] with regard to resolution level, with the mesh for Geometry A containing approximately 2.8 M tetrahedral cells. Note that a fully unstructured (tetrahedral) mesh was used rather than a hybrid mesh containing a structured boundary layer region near the walls. This approach was found by the authors to be satisfactory for simulations in an idealized airway geometry [12,16], i.e., identical airway resistances were obtained for grid independent meshes of either type. For ease of construction, the fully tetrahedral approach is adopted here. Grid independence was verified by running steady-state simulations on a much finer grid (~36 M cells) for a comparable test case, and no appreciable change in alveolar pressure profile was observed for a given flow rate. The grid resolution level is illustrated graphically in Fig. 7, which shows the triangular surface mesh in the region of the oral cavity and near one of the distal boundaries.

Simulation Methodology

Numerical Details. The commercial software package ANSYS FLUENT®, v. 14.0 (ANSYS, Inc., Canonsburg, PA) was used to perform the simulations. Laminar flow was assumed for the entire flowfield throughout the entire breathing cycle. This assumption may not strictly hold, especially in the orotracheal region during

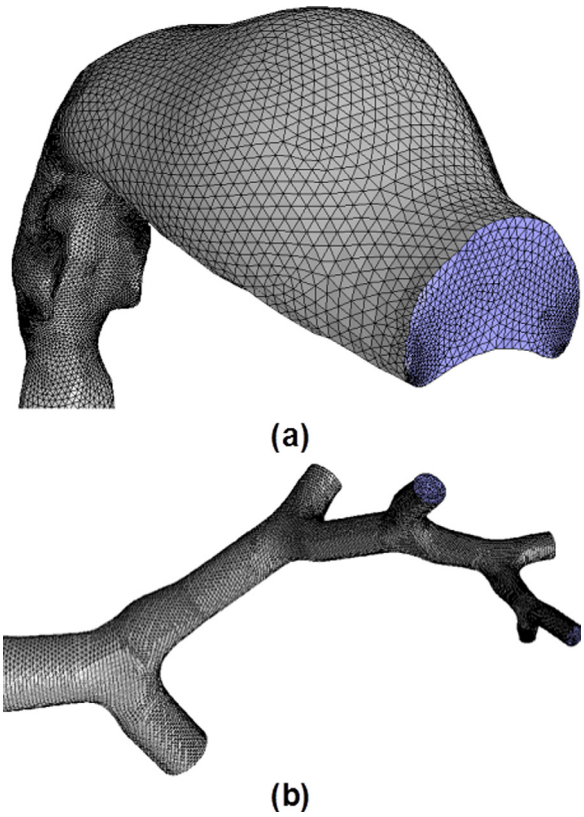

Fig. 7 Illustration of surface mesh used in the present study: (*a*) oral cavity and larynx and (*b*) vicinity of terminal boundary

maximum rates of inhalation and exhalation. However, it has been shown that the effect of a turbulence model for simulations of upper airway flow is relatively minor in comparison with the effect of boundary conditions [33], and several other prior simulations have obtained good results using laminar flow (e.g., [17,25]).

The working fluid was air with assumed constant density ($\rho = 1.225\,\text{kg/m}^3$) and viscosity ($\mu = 1.7894 \times 10^{-5}\,\text{kg/m s}$). Second-order upwind discretization was used for convective terms in the momentum equations, second-order central differencing was used for diffusive terms, the PRESTO scheme was used for discretization of the pressure, and the SIMPLE scheme was used for pressure velocity coupling. Unsteady terms were discretized using a second-order two-point backward difference approximation.

The simulations for the validation test case were based on a breathing period of 5 s, and used 200 equally spaced time steps ($\Delta T = 0.025$ s) per breath cycle. This choice was based on a previous study using a comparable geometry and mesh resolution level [27]. Simulations performed with a 50% smaller time step size were shown to yield no appreciable differences in the results. Because the solution algorithm was implicit, it was necessary to converge the solution at each time step. It was found that 150 iterations were required at each time step to ensure convergence, which was judged based on a reduction of the mass flow imbalance to less than 0.01% of the mass flow at the oral boundary, and a reduction of three orders of magnitude in the L_2 norm of the momentum equation residual during the time step.

No-slip conditions were applied at wall boundaries. A constant total pressure of 0 Pa (gauge) was applied at the oral opening. In FLUENT, the prescribed pressure is automatically applied as a total pressure condition for flow into the domain (i.e., during inhalation) and a static pressure condition for flow out of the domain (i.e., during exhalation). All distal flow boundaries (truncated and terminal) were specified using a prescribed time-dependent velocity. The value of the velocity at each time step and at each distal boundary was specified to yield a specific volumetric flow rate. The flow rate was defined for each boundary as some fraction of the overall target flow rate into (or out of) the oral opening. The methods for specifying the overall flow rate and the fractional distal flow rate distribution are described in detail in the following two sections.

Breathing Input Data. It was desired to use physiologically realistic ventilation profiles for the simulations. Significant patient-to-patient variation is seen in actual breathing patterns due to differences in size, gender, age, weight, etc., acute and chronic pathophysiological conditions, environmental conditions, and activity levels. Even under idealized conditions with nominally identical subjects, differences among sample populations are observed.

Statistically relevant ventilation profiles were obtained using the HumMod whole-body human physiology model [34]. HumMod is an integrative model of human physiology that includes approximately 5100 physiological variables and 242 ordinary differential equations describing a variety of physiological responses. The underlying HumMod algorithm is based on meta-analysis of documented experimental studies describing specific physiological mechanisms, and the current version includes information from over 5900 different source references. Development of HumMod began at the University of Mississippi Medical Center in the 1960s [35] and the model has undergone multiple revisions in which additional functionality has been incorporated and validated.

The HumMod predicted ventilation pattern for a healthy, middle-aged male under resting conditions is shown in Fig. 8, in terms of inhaled air volume versus time. Lung volume is expressed in liters (L) relative to a functional residual capacity of 2.57 L. The tabular volume data was supplied by HumMod with a

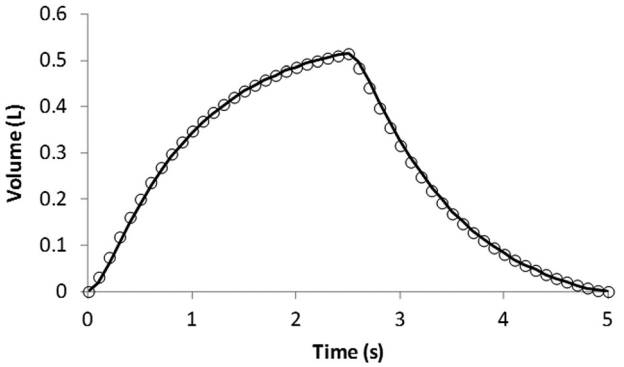

Fig. 8 Ventilation profile provided by HumMod (symbols) and obtained by integration of the prescribed volumetric flow rate (*Q*) profile shown in Fig. 9 (solid line)

time increment of 0.1 s over a cyclic period of 5 s. A corresponding volumetric flow rate (Q) profile was obtained by numerically differentiating the volume data with respect to time. Central differencing was used at each point in the profile, with the exception of the maximum and minimum volume states corresponding to the beginning of inspiration and expiration, respectively. At those points the volumetric flow rate was assumed to be zero. The resulting Q profile was then numerically integrated over the inhalation phase using trapezoid rule and the resulting maximum volume was calculated. The values of Q over the inhalation phase were then adjusted (multiplied by a constant value) to ensure that the volumetric flow rate profile used in the simulations would accurately reproduce the total increase in air volume during the inhalation phase. An analogous procedure was used to adjust the volumetric flow rate profile during the exhalation phase, to ensure that the integrated lung volume returned to zero after one complete breathing cycle. The resulting time-dependent flow rate distribution is shown in Fig. 9. The integrated volume curve obtained from that Q profile is shown in Fig. 8, and shows good agreement with the volume profile provided by HumMod.

Unsteady Boundary Condition Specification. The time-dependent volumetric flow rate at each distal boundary i was specified as a constant fraction (α_i) of the total flow rate (Q) shown in Fig. 9. The velocity boundary condition V_i at each boundary (both truncated and terminal) was then specified according to

$$V_i(t) = \alpha_i Q(t)/A_i \tag{1}$$

where A_i is the area of boundary surface i.

The distal boundaries correspond to flow outlets during the inhalation phase and inlets during the exhalation phase of the

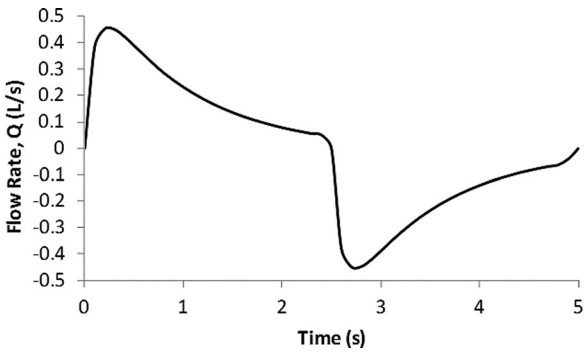

Fig. 9 Total volumetric flow rate (*Q*) profile used to apply time-dependent distal boundary conditions

breath cycle. The simplest approach is to assume that the flow rate is evenly split at each airway bifurcation, which yields a simple generational dependence defined by

$$\alpha_i = Q/2^{G_i} \tag{2}$$

where G_i represents the airway generation number for boundary i, with $G = 0$ corresponding to the trachea, and $G = 15$ corresponding to the terminal boundaries of the conducting zone.

In real lung airway flows, the flow distribution is not evenly split at each bifurcation. As seen in Fig. 5, the diameter and branching angle of paired daughter branches can be markedly different, leading to an asymmetric flow distribution. Such asymmetric flow distribution in daughter branches for realistic airway branching has been clearly demonstrated in simulations of small-scale regions of the bronchial network [36].

Physiologically, air flow is driven by the pressure difference between the oral opening and the alveoli. The alveolar pressure (P_{alv}) is related to the time varying pleural pressure (P_{pl}) and the transpulmonary pressure (P_{tp}) by

$$P_{alv} = P_{pl} + P_{tp} \tag{3}$$

Except in cases of severe pathophysiological conditions such as pneumothorax, the pressure in the pleural space exhibits only a relatively small spatial gradient due to the effect of gravity [37]. For the purposes of this study, the gravity induced gradient is assumed to be zero, i.e., spatially uniform pleural pressure. The transpulmonary pressure is a function of the inhaled lung volume, and arises due to the elastic recoil of the lungs and chest cavity. It is also assumed to be spatially uniform throughout the lung volume. For healthy breathing, then, it is expected that alveolar pressure, though time varying, is approximately uniform throughout the lung. Because the resistance of the pulmonary zone is small relative to the conducting zone [38], we assume for simulation purposes that the terminal boundary pressure is equal to the alveolar pressure and spatially uniform.

Based on the above considerations, it is desired to specify the distal boundary flow distribution fractions α_i such that the pressure distribution at terminal boundaries is approximately uniform, and pressures at the truncated boundaries are physiologically realistic. A simple method was adopted in this study, for which the outlet boundary mass flow distribution fractions α_i were set equal in the unsteady breathing cases to values that were obtained from a preliminary steady-state simulation. For the steady-state simulation, the constant inlet mass flow rate was set as the average flow rate during one inhalation cycle. For the present study, the inhaled air volume is 0.515 L, over an inhalation time of 2.5 s (Fig. 8). The average volumetric flow rate is therefore $Q_{avg} = 0.206$ L/s, and this value was applied using a mass flow inlet boundary condition at the oral opening.

In the preliminary steady-state simulation, a pressure boundary condition was specified at the distal boundaries, with terminal outlet pressures set equal to zero (gauge), and values of pressure at truncated outlets assigned using the stochastic coupling approach first documented in Ref. [12]. In this approach, interior airway face zones in a given airway generation are randomly associated with truncated outlet boundaries in the same generation. Pressures are therefore not assigned a priori to truncated boundaries, but instead, as the simulation proceeds, the averaged pressures at interior face zones are mapped to their corresponding outlet zones. The pressure outlet conditions therefore converge to physiologically realistic values as the simulation converges to a steady-state solution, with no requirement to estimate the pressure or flow rate at the truncated boundaries prior to the simulation. For further details the reader is referred to Refs. [12,16,17]. Once a converged steady-state solution was obtained, the fraction of inlet flow through each of the terminal and truncated outlet boundaries was calculated and set as α_i, and these values were used during the unsteady breathing simulations.

Results and Discussion

Results are first presented from unsteady breathing simulations using the total volumetric flow rate shown in Fig. 9. The results are analyzed in terms of the time-dependent inhaled air volume, the time-dependent pressures at the distal boundaries, and the spatial distribution of pressure in the lung airway domain. For each simulation, three complete breathing cycles were run. It was determined that the flow was periodic after one cycle, i.e., no differences were observed between the second and third cycles. All results shown below are from the second breath cycle.

Figure 10 shows the resulting inhaled air volume versus time as predicted by the CFD simulation. As expected, the inhaled volume agrees almost exactly with the values provided by HumMod, verifying that the method discussed above for determining the time varying total flow rate (differentiation followed by a correction to ensure the correct inhaled volume at the end of inhalation and exhalation phases) is appropriate. The simulation results also confirmed that the method yielded excellent mass conservation over each complete breath cycle, with a maximum cyclic residual volume of 8×10^{-5} L, which represents an error of less than 0.02% of the maximum inhaled volume.

Figure 11 shows the predicted average alveolar pressure, based on the previously discussed assumption of negligible pressure drop through the pulmonary zone (i.e., pressure shown is terminal bronchiole pressure), from the simulations using Geometry A. The result is compared to the HumMod predicted data for alveolar pressure, which represents a correlation based on an aggregate of experimental studies found in the literature. As seen in Fig. 11(*a*), the CFD results agree very well with HumMod, with the biggest disagreement occurring during peak inhalation and exhalation. Figure 11(*b*) includes results using Geometry B, which suffered from physiologically unrealistic anatomical features in the distal regions (Fig. 6), most notably too large length-to-diameter ratios for the lower airway branches. Geometry A, based on statistically accurate morphological parameters, yields a result in much better agreement with HumMod data and expected pressure levels.

Also shown in Fig. 11 in the form of the dotted curves are upper and lower bounds on alveolar pressure, obtained from the experimental study of DuBois et al. [39]. Measurements in that study were presented in terms of a linear airway resistance during breathing, with volumetric flow rates (Q) in the range 0–0.5 L/s. Twenty-two separate measurements were obtained from 15 different male subjects (for seven subjects measurements were taken on two different days), with an age range of 28–57 years. The study was therefore chosen as a representative sample corresponding to the current computational subject in terms of anatomical and ventilatory parameters. The curves shown in the figure represent the

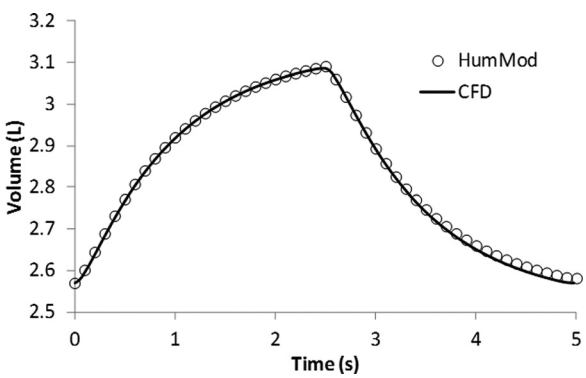

Fig. 10 Predicted lung air volume from the CFD simulation compared to the HumMod ventilation profile

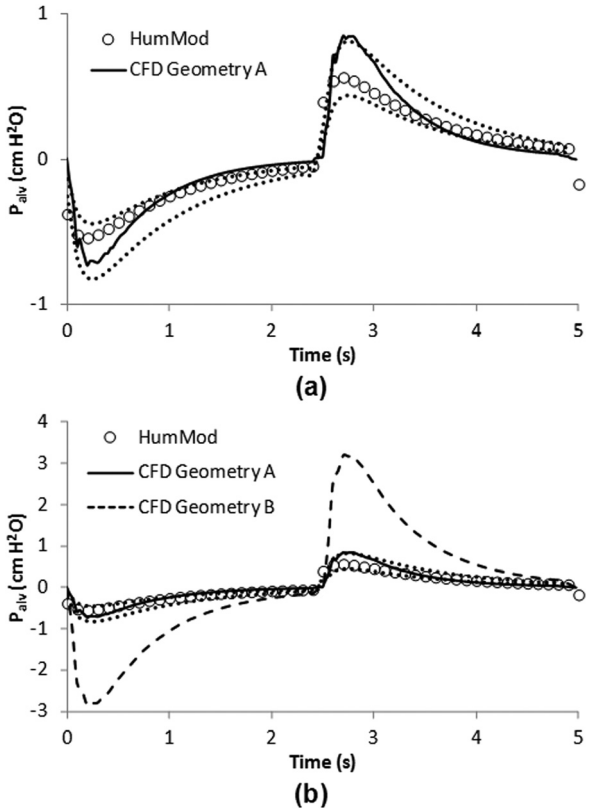

Fig. 11 Predicted unsteady pressure variation compared to HumMod data: (*a*) current simulation and (*b*) current simulation and previous simulation with less accurate computational geometry. The dotted curves represent a statistical upper and lower bound from experimental data in Ref. [39].

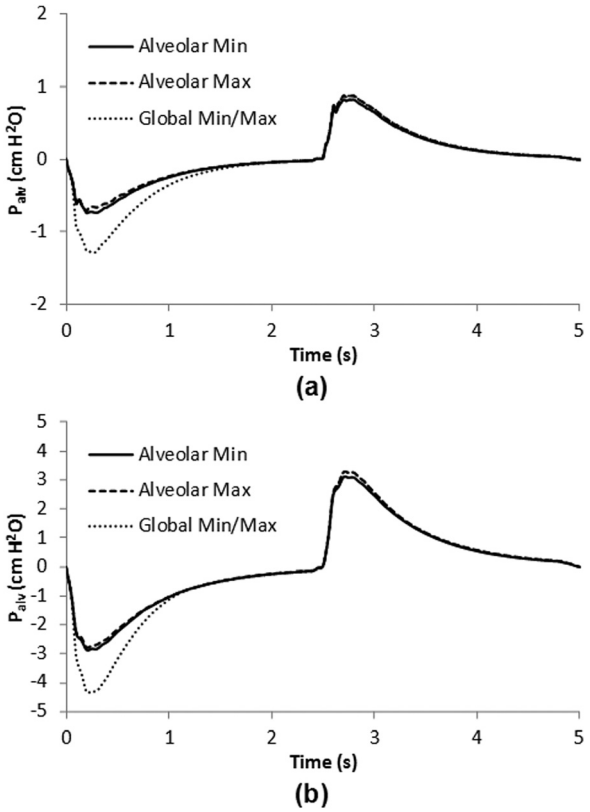

Fig. 12 Predicted unsteady pressure variation for (*a*) Geometry A and (*b*) Geometry B, showing the maximum and minimum predicted alveolar pressures, and the global minimum (inhalation) and maximum (exhalation) pressures

alveolar pressure based on an upper and lower bound of airway resistance, corresponding to the mean value obtained in Ref. [39], plus or minus one standard deviation. It is therefore expected that these bounds would include approximately 68% of the subjects studied in Ref. [39]. As shown in Fig. 11(*a*), both the HumMod predictions and the CFD results using Geometry A lie within or close to the bounds from the experimental data. It should be noted that the reproduction of alveolar pressure from Ref. [39] assumes a constant airway resistance throughout the breathing cycle, whereas the HumMod and CFD results show nonlinear behavior, i.e., variable resistance during breathing. Taking these differences into account, the agreement appears to be quite satisfactory. The results from Geometry B, on the other hand, lie well outside the bounds established by the experimental data, and indeed can be judged to be physically unrealistic as representative of alveolar pressure in a healthy human male. On the whole, the results in Fig. 11 help to provide validation evidence for both the technique used to create Geometry A and the method used to apply the time-dependent boundary conditions for the CFD simulations.

It should be noted that in addition to subject-to-subject variations, there remain modeling issues that could lead to differences between the CFD results and real breathing dynamics. One example is the potential for turbulent flow in the upper airway region for moderate to high inhalation and exhalation rates. This is considered in more detail below. Another potential source of error is the assumption of rigid airway walls, rather than the compliant walls present in real lung air flow. Xia et al. [40] recently demonstrated significant variations in maximum wall shear stress and air flow rate and distribution when comparing simulations of a rigid airway and a flexible airway using fluid–structure interaction modeling. Future work will seek to investigate and effectively resolve these issues in order to refine the approach shown here.

Figure 12 shows the time variation of the terminal boundary pressures along with the peak pressures (minimum pressure during inhalation, maximum pressure during exhalation) in the domain. Of all the terminal boundaries at G15, only the maximum and minimum pressures are shown, with all others lying within those bounds. The extent of variation between the terminal boundary pressure and peak pressure gives an indication of the level of physiological realism for the boundary condition approach. Note that the terminal pressures represent global extrema for most of the breathing cycle, with the exception of the early stage of inhalation. The reason for the disagreement in this region is that the globally minimum pressure does not occur at the terminal bronchioles, but in the larynx, due to the constriction of the flow and the relatively high volumetric flow rate. The figure also shows that the pressures do not display a wide range of variation, meaning that the distal pressure distribution is almost uniform, in agreement with actual physiological characteristics. This is observed to be true regardless of the anatomical accuracy of the airway geometry, as indicated by a comparison of Figs. 12(*a*) and 12(*b*). The pressure levels themselves, of course, are quite different between the two airway model geometries.

Figures 13 and 14 show the distribution of pressure on the airway wall at approximately peak inhalation and exhalation, respectively, for Geometry A. During inhalation, low pressure at the terminal boundaries drives the flow, however the global minimum of pressure at the larynx due to local flow acceleration is apparent. During exhalation, high pressure at the terminal boundaries drives the flow. The performance of the boundary condition methodology is highlighted in Fig. 15, which shows the pressure contours at the same instant as Fig. 14, but with the contour range reduced to highlight the pressure distribution in the bronchi and bronchiole regions. It is apparent from the figure that the truncated boundaries upstream of the terminal generation maintain pressures

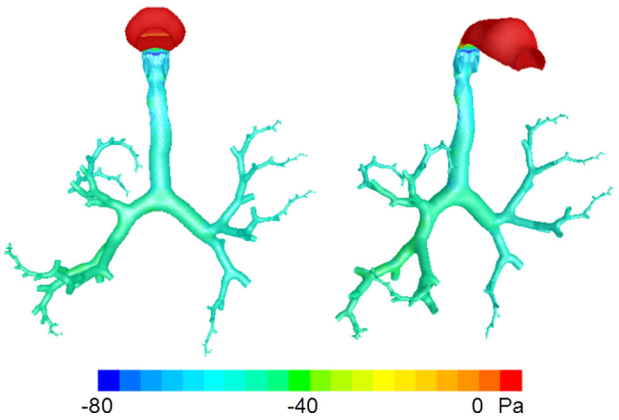

Fig. 13 Pressure contours on airway wall during inhalation

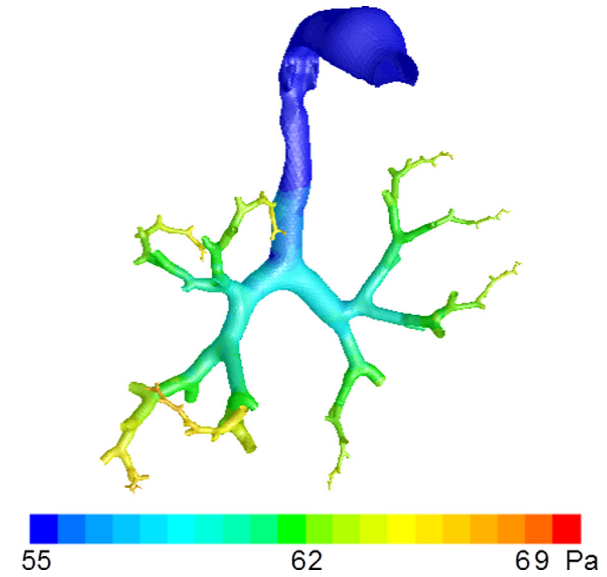

Fig. 15 Pressure contours on airway wall during exhalation, reduced contour range relative to Fig. 14

that are comparable to other generationally equivalent locations in the domain. This is due to the use of the stochastically coupled boundary condition approach in the preliminary steady state simulation to determine the mass flow fractions in the unsteady simulation. The apparently physiologically realistic distributions of pressure in the current study are significantly better than those observed in our previous study (cf. [27]), in which the fractional flow distribution at the distal boundaries was specified according to simple a priori estimates, rather than obtained from a preliminary steady state simulation.

In order to investigate the viability of a laminar flow assumption throughout the entire domain, test simulations were performed under identical conditions as those above, assuming fully turbulent flow and adopting the k-ω SST model [41] for unsteady RANS simulation. Uniform inlet boundary conditions for the turbulence variables k and ω were applied at the oral opening during the inhalation portion of the breath cycle, and applied at the terminal and truncated boundaries during exhalation. For the former, turbulence conditions were approximated using an assumption of 2% turbulence intensity, based on the average inhalation velocity, and an integral length scale of 0.005 m. The resulting boundary condition values were $k = 2 \times 10^{-4}$ m^2/s^2 and $\omega = 5$ s^{-1}. At the distal boundaries, during exhalation, low turbulence levels were assumed with boundary condition values of $k = 1 \times 10^{-5}$ m^2/s^2 and $\omega = 5$ s^{-1}.

Turbulent flow results are shown along with the laminar case in Fig. 16. It is apparent that the inclusion of a turbulence model has little effect on the pressure drop during inhalation or exhalation. A small difference is visible in the plot during near peak exhalation, but results are almost identical to the laminar case elsewhere in the breathing cycle. The relatively small significance due to turbulent versus laminar flow shown here is in agreement with previous studies in the literature [17,25,33]. It should be noted, however, that turbulent versus laminar flow may be significant with regard to other results relevant to lung airflow; for example prediction of particle and aerosol deposition in the upper airways. In addition, the turbulent flow in the tracheobronchial region of the lung occurs at lower Reynolds numbers and is qualitatively different than more the more typical shear-driven or boundary layer turbulence for which most Reynolds-Averaged Navier–Stokes (RANS) turbulence models are developed. More accurate simulations of unsteady airflow may require the use of more advanced methods such as large-eddy simulation (LES) or hybrid RANS-LES turbulence models [42–44].

Finally, to further demonstrate the capability of the computational method, additional simulations were performed using different prescribed ventilatory profiles than the one used in the validation test case above. Three profiles were obtained from the HumMod software under varying physiological conditions, for the representative subject of a healthy middle-aged male. The profiles were obtained by changing model inputs such as physiological stressors and activity level. For purposes of presentation, the three profiles are simply denoted as normal, fast and shallow, and slow and deep. Figure 17 shows the results from these simulations for all three cases, comparing the HumMod predicted pressures with results from the CFD simulations using Geometry A. It is apparent that the CFD results show very good agreement with the

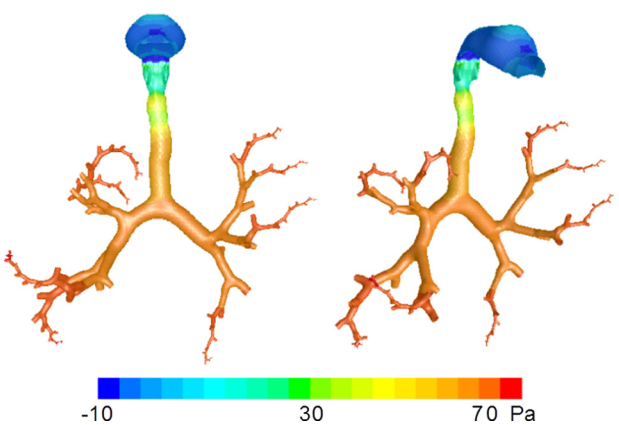

Fig. 14 Pressure contours on airway wall during exhalation

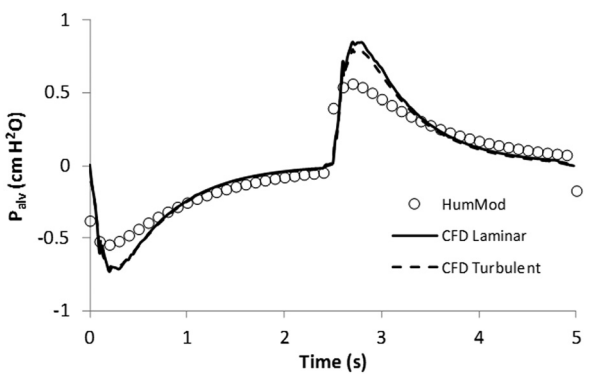

Fig. 16 Predicted unsteady alveolar pressure variation compared with HumMod data, using laminar flow model and RANS turbulence model (k-ω SST)

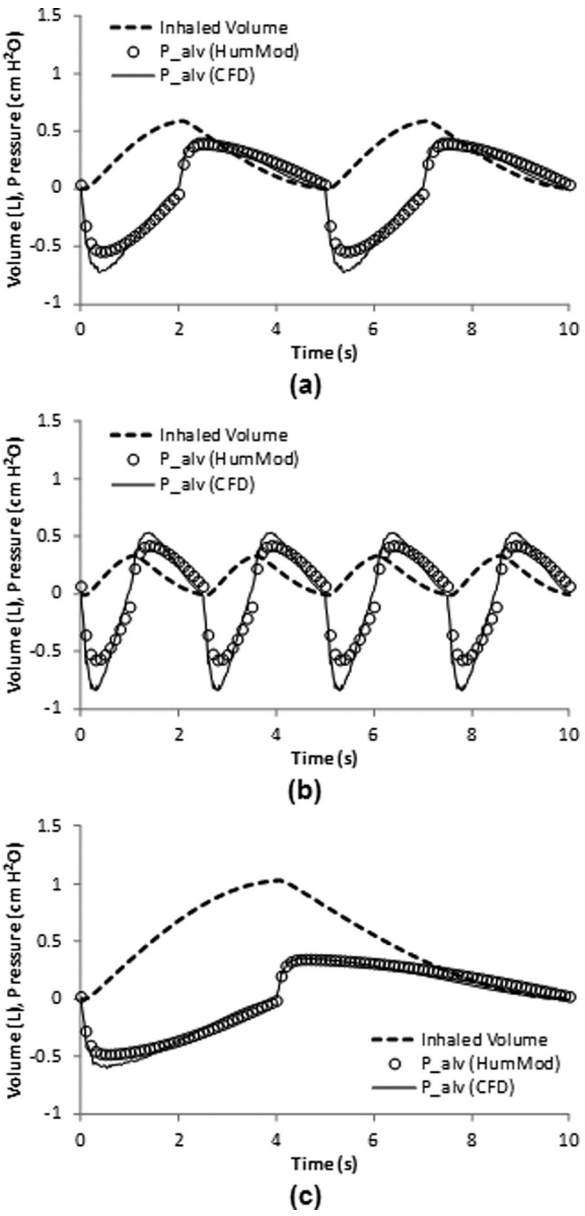

Fig. 17 Prescribed inhaled air volume profile and alveolar pressure predicted by HumMod and by CFD simulations with Geometry A. Results are shown for different activity levels leading to three different physiological states denoted as (*a*) normal, (*b*) fast and shallow, and (*c*) slow and deep.

HumMod data for all three profiles. As for the case presented above, the greatest disagreement occurs during times of peak inhalation or exhalation rate. These results help to reinforce the generality of the method for application to models of healthy human subjects, for purposes of alveolar pressure prediction.

Conclusion

Results were presented for CFD simulations of cyclic breathing in the human lung. Key features of the simulations include: (1) a physiologically realistic computational geometry based on CT imaging of the upper airways and a space-filling tree algorithm with statistically accurate morphological parameters for the lower airways; (2) generation of a reduced geometry approximate model via truncation of selected airways; (3) accurate treatment of time-dependent distal boundary conditions; and (4) use of physiologically accurate ventilatory parameters obtained from the whole-body simulation software HumMod. The use of a truncated geometry to represent the conducting zone (up to the 16th generation) resulted in a computational model that reduces the computational expense by 99.5% versus an equivalent fully resolved geometry.

The simulations presented here represent the further evolution of a method for lung flow simulation that has been previously developed by the authors in Refs. [12,16,17,27]. The primary contribution in this paper is the development of a physiologically realistic method for prescribing flow distribution in the terminal and truncated outlets, based on a steady state preliminary simulation using stochastically coupled pressure boundary conditions. The method is simple to implement, and requires only the airway geometry and target inhaled air volume profile, with no need to estimate airway pressures at distal boundaries using one-dimensional or impedance-based approximations, and no need to prescribe the distal mass flow or pressure distribution a priori.

The methodology presented here uses a prescribed time-dependent flow rate during the breath cycle as an input. Results show that the simulations are capable of reproducing a realistic terminal (alveolar) pressure profile, in good agreement with the profile provided by HumMod, which is based on correlation of aggregated experimental data available in the literature, and on a specific experimental study using test subjects representative of the computational analog [39]. Furthermore, the method shows a nearly uniform distribution of distal pressure, and conserves mass over the inhale–exhale cycle. Comparisons between two different computational geometries highlight the importance of using a morphologically accurate geometry for the upper and lower airway region, if quantitatively accurate results are to be obtained. The results also reinforce previous conclusions that the reduced geometry approach used here can be a viable alternative to simulations that employ fully resolved airway geometries, reducing computational expense by orders of magnitude while providing comparable accuracy and three-dimensional resolution of the airflow throughout all 16 generations of the conducting zone. Research efforts are currently underway to extend the airway tree through the pulmonary zone and incorporate alveolar structure and motion into the simulations.

Acknowledgment

This research was funded by the National Science Foundation under Grant No. EPS-0903787.

References

[1] Choi, J., Tahwai, M. H., Hoffman, E. A., and Lin, C.-L., 2009, "On Intra- and Inter-Subject Variabilities of Airflow in the Human Lungs," Phys. Fluids, **21**, p. 101901.
[2] Vial, L., Perchet, D., Fodil, R., Caillibotte, G., Fetita, C., Preteux, F., Beigelman-Aubry, C., Grenier, P., Thiriet, M., Isabey, D., and Sbirlea-Apiou, G., 2005, "Airflow Modeling of Steady Inspiration in Two Realistic Proximal Airway Trees Reconstructed From Human Thoracic Tomodensitometric Images," Comput. Meth. Biomech. Biomed. Eng., **8**, pp. 267–277.
[3] Tawhai, M. H., Pullan, A. J., and Hunter, P. J., 2000, "Generation of an Anatomically Based Three-Dimensional Model of the Conducting Airways," Ann. Biomed. Eng., **28**, pp. 793–802.
[4] van Ertbruggen, C., Hirsch, C., and Paiva, M., 2005 "Anatomically Based Three-Dimensional Model of Airways to Simulate Flow and Particle Transport Using Computational Fluid Dynamics," J. Appl. Phys., **98**, pp. 970–980.
[5] Tena, A. F., Casan, P., Marcos, A., Barrio, R., and Blanco, E., 2011, "Analysis of the Fluid Dynamic Characteristics of the Obstructive Pulmonary Diseases Using a Three-Dimensional CFD Model of the Upper Conductive-Zone of the Lung Airways," Proceedings of the ECCOMAS Thematic International Conference on Simulation and Modeling of Biological Flows.
[6] Tian, L., and Ahmadi, G., 2012, "Transport and Deposition of Micro- and Nano-Particles in Human Tracheobronchial Tree by an Asymmetric Multi-Level Bifurcation Model," J. Comp. Multiphase Flows, **4**, pp. 159–182.
[7] Leary, D., Bhatawadekar, S. A., Parraga, G., and Maksym, G. N., 2012, "Modeling Stochastic and Spatial Heterogeneity in a Human Airway Tree to Determine Variation in Respiratory System Resistance," J. Appl. Physiol., **112**, pp. 167–175.
[8] Goo, J., and Kim, C. S., 2003, "Theoretical Analysis of Particle Deposition in Human Lungs Considering Stochastic Variations of Airway Morphology," J. Aerosol. Sci., **34**, pp. 585–602.

[9] Asgharian, B., and Price, O. T., 2007, "Deposition of Ultrafine (NANO) Particles in the Human Lung," Inhal. Toxicol., **19**, pp. 1045–1054.
[10] Ma, B., and Darquenne, C., 2011, "Aerosol Deposition Characteristics in Distal Acinar Airways Under Cyclic Breathing Conditions," J. Appl. Physiol., 110, pp. 1271–1282.
[11] Yin, Y., Choi, J., Hoffman, E. A., Tawhai, M. H., and Lin, C.-L., 2010, "Simulation of Pulmonary Air Flow With a Subject-Specific Boundary Condition," J. Biomech., **43**, pp. 2159–2163.
[12] Walters, D. K., and Luke, W. H., 2010, "A Method for Three-Dimensional Navier–Stokes Simulations of Large-Scale Regions of the Human Lung Airway," ASME J. Fluids Eng., **132**(5), p. 051101.
[13] Tawhai, M. H., and Lin, C.-L., 2010, "Image-Based Modeling of Lung Structure and Function," J. Magn. Reson. Imaging, **32**, pp. 1421–1431.
[14] Nowak, N., Kadake, P. P., and Annapragada, A. V., 2003, "Computational Fluid Dynamics Simulation of Airflow and Aerosol Deposition in Human Lungs," Ann. Biomed. Eng., **31**, pp. 374–390.
[15] Zhang, Z., Kleinstreuer, C., and Kim C. S., 2008, "Airflow and Nanoparticle Deposition in a 16-Generation Tracheobronchial Airway Model," Ann. Biomed. Eng., **36**, pp. 2095–2110.
[16] Walters, D. K., and Luke, W. H., 2011, "Computational Fluid Dynamics Simulations of Particle Deposition in Large-Scale, Multi-Generational Lung Models," ASME J. Biomech. Eng., **133**(1), p. 011003.
[17] Walters, D. K., Burgreen, G. W., Lavallee, D. M., Thompson, D. S., and Hester, R. L., 2011, "Efficient, Physiologically Realistic Lung Airflow Simulations," IEEE Trans. Biomed. Eng., **58**, pp. 3016–3019.
[18] Tian, G., Longest, P. W., Su, G., Walenga, R. L., and Hindle, M., 2011, "Development of a Stochastic Individual Path (SIP) Model for Predicting the Tracheobronchial Deposition of Pharmaceutical Aerosols: Effects of Transient Inhalation and Sampling the Airways," J. Aerosol Sci., **42**, pp. 781–799.
[19] Longest, P. W., Tian, G., Walenga, R. L., and Hindle, M., 2012, "Comparing MDI and DPI Aerosol Deposition Using in Vitro Experiments and a New Stochastic Individual Path (SIP) Model of the Conducting Airways," Pharm. Res., **9**(6), pp. 1670–1688.
[20] Tian, G., Longest, P. W., Su, G., and Hindle, M., 2011, "Characterization of Respiratory Drug Delivery With Enhanced Condensational Growth Using an Individual Path Model of the Entire Tracheobronchial Airways," Ann. Biomed. Eng., **39**, pp. 1136–1153.
[21] Tena, A. M., Casan, P., Fernandez, J., Ferrera, C., and Marcos, A., 2013, "Characterization of Particle Deposition in a Lung Model Using an Individual Path," EPJ Web Conf., **45**, pp. 1–5.
[22] Weibel, E. R., 1963, *Morphometry of the Human Lung*, Academic, New York.
[23] Gemci, T., Ponyavin, V., Chen, Y., Chen, H., and Collins, R., 2008, "Computational Model of Airflow in Upper 17 Generations of Human Respiratory Tract," J. Biomech., **41**, pp. 2047–2054.
[24] De Backer, J. W., Vos, W. G., Vinchurkar, S. C., Claes, R., Drollman, A., Wulfrank, D., Parizel, P. M., Germonpre, P., and De Backer, W., 2010, "Validation of Computational Fluid Dynamics in CT-Based Airway Models With SPECT/CT," Radiology, **257**, pp. 854–862.
[25] Ma, B., and Lutchen, K. R., 2006, "An Anatomically Based Hybrid Computational Model of the Human Lung and Its Application to Low Frequency Oscillatory Mechanics," Ann. Biomed. Eng., **34**, pp. 1691–1704.
[26] Malve, M., Chandra, S., Lopez-Villalobos, J. L., Finol, E. A., Ginel, A., and Doblare, M., 2012, "CFD Analysis of the Human Airways Under Impedance-Based Boundary Conditions: Application to Healthy, Diseased and Stented Trachea," Comp. Meth. Biomech. Biomed. Eng., **16**(2), pp. 198–216.
[27] Walters, D. K., Burgreen, G. W., Hester, R. L., Thompson, D. S., Lavallee, D. M., Pruett, W. A., and Ford-Green, J., 2012, "Simulations of Cyclic Breathing in the Conducting Zone of the Human Lung," ASME Paper No. FEDSM2012-72474.
[28] Gaither, J. A., Marcum, D. L., and Mitchell, B., 2000, "SolidMesh: A Solid Modeling Approach to Unstructured Grid Generation," Proceedings of the 7th International Conference on Numerical Grid Generation in Computational Field Simulations, Whistler, Canada.
[29] Kitaoka, H., Takaki, R., and Suki, B., 1999, "A Three Dimensional Model for Human Airway Tree," J Appl. Physiol., **76**, pp. 2207–2217.
[30] Tawhai, M. H., Hunter, P., Tschirren, J., Reinhardt, J., McLennan, G., and Hoffman, E. A., 2004, "CT-Based Geometry Analysis and Finite Element Models of the Human and Ovine Bronchial Tree," J Appl. Physiol., **97**, pp. 2310–2321.
[31] Yeh, H.-C., and Schum, G. M., 1980, "Models of Human Lung Airways and Their Application to Inhaled Particle Deposition," Bull. Math. Biol., **42**, pp. 461–480.
[32] Schmidt, A., Zidowitz, S., Kriete, A., Denhard, T., Krass, S., and Peitgen, H.-O., 2004, "A Digital Reference Model of the Human Bronchial Tree," Comput. Med. Imaging Graph., **28**, pp. 203–211.
[33] Longest, P. W., and Vinchurkar, S., 2007, "Validating CFD Predictions of Respiratory Aerosol Deposition: Effects of Upstream Transition and Turbulence," J. Biomech., **40**, pp. 305–316.
[34] Hester, R. L., Brown, A. J., Husband, L., Iliescu, R., Pruett, D., Summers, R., and Coleman, T. G., 2011, "HumMod: A Modeling Environment for the Simulation of Integrative Human Physiology," Frontiers Physiol., **2**(12), pp. 1–12.
[35] Guyton, A. C., and Coleman, T. G., 1969, "Quantitative Analysis of the Pathophysiology of Hypertension," Circul. Res., **24**, pp. 1–19.
[36] Soni, B., Lindley, C., and Thompson, D., 2009, "The Combined Effects of Non-Planarity and Asymmetry on Primary and Secondary Flows in the Small Bronchial Tubes," Int. J. Num. Meth. Fluids, **59**, pp. 117–146.
[37] Bryan, A. C., Milic-Emili, J., and Pengelly, D., 1966, "Effect of Gravity on the Distribution of Pulmonary Ventilation," J. Appl. Physiol., **21**, pp. 778–784.
[38] Pedley, T. J., Schroter, R. C., and Sudlow, M. F., 1970, "The Prediction of Pressure Drop and Variation of Resistance Within the Human Bronchial Airways," Resp. Physiol., **9**, pp. 387–405.
[39] DuBois, A. B., Botelho, S. Y., and Comroe, J. H., 1956, "A New Method for Measuring Airway Resistance in Man Using a Body Plethysmograph: Values in Normal Subjects and in Patients With Respiratory Disease," J. Clin. Invest., **35**, pp. 327–335.
[40] Xia, G., Tawhai, M. H., Hoffman, E. A., and Lin, C.-L., 2010, "Airway Wall Stiffening Increases Peak Wall Shear Stress: A Fluid–Structure Interaction Study in Rigid and Compliant Airways," Ann. Biomed. Eng., **38**, pp. 1836–1853.
[41] Menter, F. R., 1994, "Two-Equation Eddy-Viscosity Turbulence Models for Engineering Applications," AIAA J., **32**, pp. 1598–1605.
[42] Spalart, P. R., 2000, "Strategies for Turbulence Modelling and Simulations," Int. J. Heat Fluid Flow, **21**, pp. 252–263.
[43] Bhushan, S., and Walters, D. K., 2012, "A Dynamic Hybrid RANS/LES Modeling Framework," Phys. Fluids, **24**, p. 015103.
[44] Walters, D. K., Bhushan, S., Alam, M. F., and Thompson, D. S., 2013, "Investigation of a Dynamic Hybrid RANS/LES Modelling Methodology for Finite-Volume CFD Simulations," Flow Turbul. Combust. **91**(3), pp. 643–667.